ECS Journal of Solid State
Science and Technology

Analytical Specificity and Microbial Interference Study of a 30-Second Quantitative SARS-CoV-2 Detection Biosensor System

To cite this article: Chao-Ching Chiang *et al* 2022 *ECS J. Solid State Sci. Technol.* **11** 105007

ECS Journal of Solid State Science and Technology, 2022 **11** 105007
2162-8777/2022/11(10)/105007/6/$40.00 © 2022 The Electrochemical Society ("ECS"). Published on behalf of ECS by IOP Publishing Limited

Analytical Specificity and Microbial Interference Study of a 30-Second Quantitative SARS-CoV-2 Detection Biosensor System

Chao-Ching Chiang,[1,*,z] Chan-Wen Chiu,[1] Fan Ren,[1,] Cheng-Tse Tsai,[2] Yu-Te Liao,[2] Josephine F. Esquivel-Upshaw,[3] and Stephen J. Pearton[4,**]**

[1]*Department of Chemical Engineering, University of Florida, Gainesville, Florida 32611, United States of America*
[2]*Department of Electronics and Electrical Engineering, National Yang Ming Chiao Tung University, Hsinchu 30010, Taiwan*
[3]*Department of Restorative Dental Sciences, Division of Prosthodontics, University of Florida, Gainesville, Florida 32610, United States of America*
[4]*Department of Materials Science and Engineering, University of Florida, Gainesville, Florida 32611, United States of America*

The analytical specificity and microbial interference of a SARS-CoV-2 biosensor detection platform were elucidated in this work. A cost-effective and highly sensitive detection system for the virus has been developed with the capability of producing quantitative results comparable with polymerase chain reaction (PCR) within 30 s. This could meet the demand for a fast diagnosis solution needed for the ongoing global pandemic. Disposable strips were biofunctionalized and immobilized with monoclonal SARS-CoV-2 antibodies. A printed circuit board embedded with a metal–oxide–semiconductor field-effect transistor (MOSFET) was also designed. The strips were connected to the gate electrode of the MOSFET, which received a synchronous pulse along with the drain electrode. The resulting waveform from the drain was then converted to digital readouts corresponding to virus or spike protein concentrations. We investigated 26 common organisms which are likely presented in the respiratory system along with 5 pathogens from the same genetic family of the SARS-CoV-2 virus for having cross-reaction or microbial interference, either of which would hinder the efficacy of the system. None of these organisms decreased the virus detection effectiveness of the sensor system.
 [DOI: 10.1149/2162-8777/ac9b8f]

Manuscript submitted July 4, 2022; revised manuscript received September 11, 2022. Published October 31, 2022.

The global pandemic of the SARS-CoV-2 virus has taken 6.3 million lives worldwide and led to economic and societal dislocation. The mutation of different variants of the virus is an ongoing process and makes treatment for the disease a challenge. Omicron variants, namely the lineages BA.1, BA.1.1, and BA.2 are currently the most common variants. According to the Centers for Disease Control and Prevention (CDC) and World Health Organization (WHO), 230 million confirmed cases have been recorded since the Omicron variant showed up at the end of 2021, which has contributed to nearly half of the accumulated cases in history. To cope with the skyrocketing infection rates and costly mitigation policies, such as quarantine, vaccinations, and frequent testing, fast, precise, and cost-effective detection solutions are urgently needed to relieve the burden on state and federal agencies.

Various virus detection methods have been developed throughout the pandemic. The most common are the polymerase chain reaction (PCR) and lateral flow antigen tests.[1] Although PCR can provide quantitative results with high specificity and sensitivity, the requirement of specific lab equipment and long processing time makes it difficult to be applied in a daily, point-of-care situation.[2,3] On the other hand, the lateral flow test offers a quick detection response from a cost-effective kit. However, due to the fact that low virus concentration could still be infectious,[4] its characteristic of low limit of detection creates a blind spot of information and increases the difficulty of reducing possible transmission.

In the race to develop novel methods to overcome the shortcomings of PCR and lateral flow tests, BioFET devices hold promise for accurate and rapid detection of the virus. Biomolecules act as a probe to replace the traditional external power source for the gate electrode and the altered molar concentration is amplified by the FET, creating an extra-low response time, miniature design, and low limit of detection system.[5] Seo et al. utilized a graphene-based BioFET along with the functionalization of PBASE (1-pyrenebutyric acid N-hydroxysuccinimide ester) to achieve a limit of detection of 1.6×10^1 pfu ml^{-1} on the cultured virus and 2.42×10^2 copies ml^{-1} on clinical samples.[6] Other types of functionalized liquid probes and implementation also developed low background noise, portable, and PCR-comparable diagnostic systems.[7–9] However, most of these are not very practical because the BioFET has to be replaced at every testing, making the reusability and versatility of this device in targeting different microbes unrealistic.

In our previous work, disposable strips were implemented as an extension of the BioFET and enabled separation of the detection mechanism from the amplification. A cost-effective, sensitive, and reconfigurable rapid detection platform was designed with a printed circuit board.[10] A double-pulse gating method was implemented to eliminate undesirable screening effects and charge accumulation.[11] Various targeted microbes such as the Zika virus, cerebrospinal fluid, and cardiac troponin I have all been detected with the same approach.[12–14] The objective of this study was to determine the possible impact of certain microorganisms in disrupting the ability of a novel sensor to detect the SARS-CoV2 virus in artificial saliva, thereby causing an interference. These organisms were selected based on the recommendations from the U.S. Food and Drug Administration (FDA) In Vitro Diagnostics Emergency Use Authorization (EUA) Guidelines for COVID detection devices.

Experimental

Commercially available disposable strips similar to glucose testing strips without the functionalized glucose enzyme were used in this study. Figure 1a illustrates an example strip. The strips were designed with carbon-printed electrodes and a microfluidic channel at the tip was plated with gold particles and bio-functionalized with SARS-CoV-2 antibodies. The electrode functionalization started with making 10 mM of thioglycolic acid (TGA) in deionized water, then applying this to the channel. The formation of Au-S bonds between Au on the electrode and the thiol functional group of TGA provided the backbone for attaching the functional groups, which target the specific antibodies. After 2 h of reaction time, the sensor strips were rinsed with deionized water and blow-dried with nitrogen. 0.1 mM N, N′-Dicyclohexylcarbodiimide (DCC) in 25% acetonitrile and 75% deionized water was applied for 1 h followed by another hour of 0.1 mM N-Hydroxysuccinimide (NHS) in deionized water. Once the reaction was completed, isopropyl

*Electrochemical Society Student Member.
**Electrochemical Society Fellow.
[z]E-mail: cchiang@ufl.edu

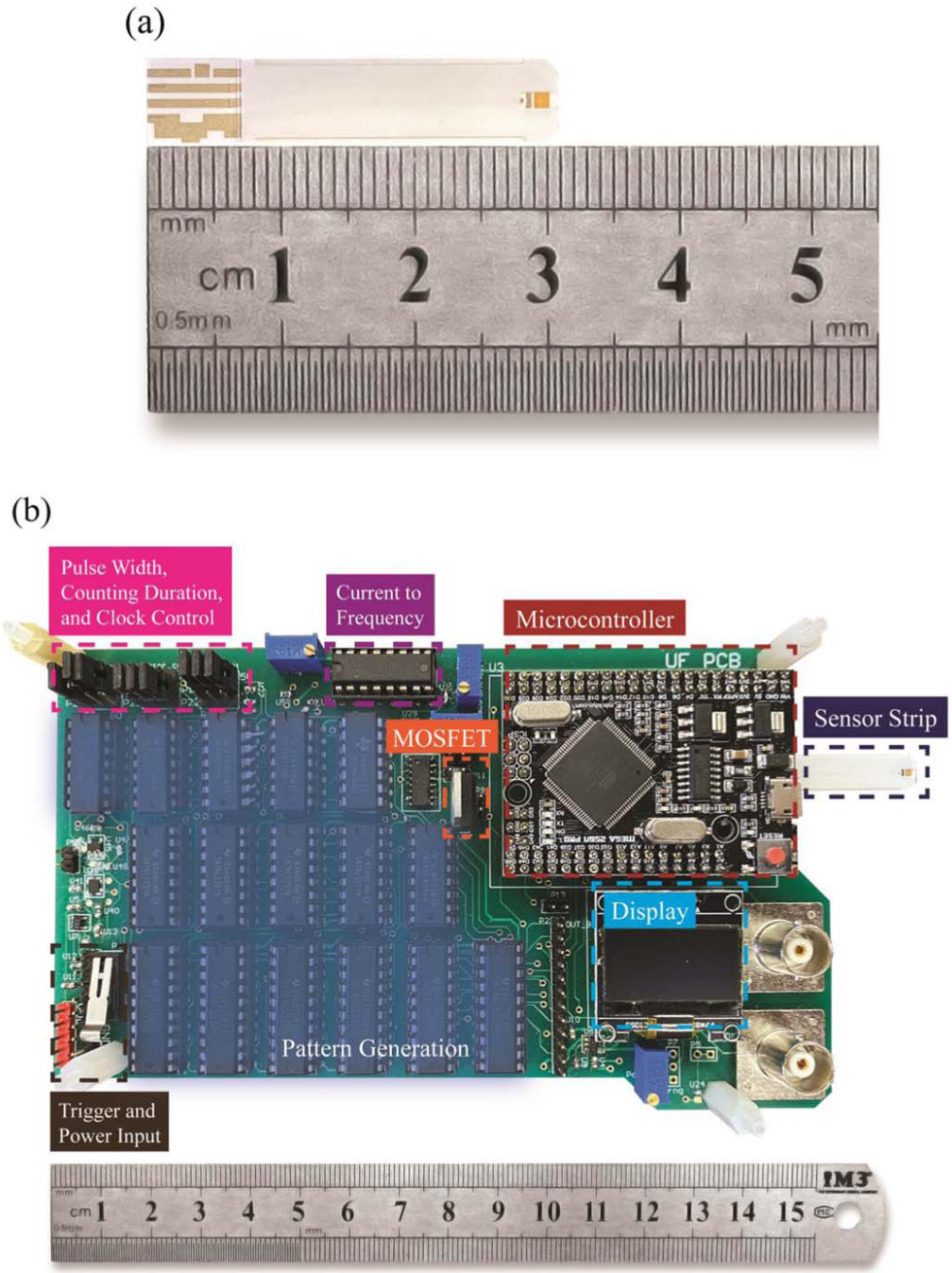

Figure 1. Schematic and photograph of the (a) testing strip and (b) testing platform including a PCB board and a test strip inserted on to the board.

alcohol, deionized water, and nitrogen gas were applied to the microfluidic channel to remove any residual liquid. Subsequently, 20 μg ml^{-1} of Anti-SARS-CoV-2 Spike Glycoprotein RBD antibody 5 g8 (Abcam, Waltham, MA) in 1% phosphate-buffered saline (PBS) was introduced into the channel. The strips were then incubated at 4 °C for 18 h. Upon completion, the functionalized sensor strips were rinsed again with 1% PBS.

A printed circuit board (PCB) with an embedded silicon MOSFET STP200N3LL (STMicroelectronics, Geneva, Switzerland) was developed to perform the detection method with the functionalized sensor strips in the previous study, as shown in Fig. 1b.[10] By design, the strip received a synchronous 1.5 V pulse pattern to the electrode functionalized with antibodies along with another synchronized 5 V to the drain electrode of the MOSFET. The induced charge changes in the microfluidic channel were then returned to the gate electrode and amplified by the MOSFET. Corresponding to the concentration of the SARS-CoV-2 virus constrained by the functionalized antibodies, the analog output waveform from the drain electrode of the transistor was then integrated with an Arduino microcontroller. For each manually triggered measurement, ten pulse patterns with 1.1 millisecond time gaps were sent and the results were averaged and displayed on the onboard LCD as a 4-digit reading.

Thirty-one (31) species of organism samples (Table I) were purchased from ATCC (Manassas, VA) and Zeptometrix (Buffalo, NY) for both analytical specificity (cross-reactivity) and microbial interference studies. This collection of organisms was selected according to the recommendation from the FDA EUA. On top of the list were 5 coronaviruses from the same generic family with SARS-CoV-2, which have a high risk of

Table I. Digital readings of cross-reactivity and microbial interference testing results.

		Cross-reactivity		Microbial interference	
Organism name	Concentration	Saliva	Organism with saliva	SARS-CoV-2	Organism with SARS-CoV-2
Adenovirus 1 Ad. 71	1.50×10^5 $TCID_{50}$ ml^{-1}	3236 ± 4	3249 ± 8	2975 ± 13	2982 ± 11
Adenovirus 2	1.50×10^5 $TCID_{50}$ ml^{-1}	3349 ± 4	3358 ± 13	3242 ± 9	3256 ± 5
Adenovirus 7a	1.50×10^5 $TCID_{50}$ ml^{-1}	3378 ± 7	3364 ± 24	3240 ± 11	3223 ± 16
Coronavirus 229E	1.50×10^5 $TCID_{50}$ ml^{-1}	3374 ± 2	3367 ± 3	3231 ± 6	3225 ± 17
Coronavirus NL63	1.50×10^5 $TCID_{50}$ ml^{-1}	3367 ± 3	3211 ± 7	3209 ± 3	3119 ± 3
Coronavirus NL63 1:10	1.50×10^4 $TCID_{50}$ ml^{-1}	3349 ± 16	3364 ± 8	3219 ± 11	3245 ± 9
Coronavirus OC43	1.50×10^5 $TCID_{50}$ ml^{-1}	3271 ± 6	3251 ± 5	3088 ± 11	3099 ± 11
Enterovirus	1.50×10^5 $TCID_{50}$ ml^{-1}	3231 ± 8	3253 ± 9	2849 ± 15	2838 ± 7
Human Metapneumovirus	1.50×10^5 $TCID_{50}$ ml^{-1}	3216 ± 10	3250 ± 5	3108 ± 22	3108 ± 26
Influenza A	1.50×10^5 $CEID_{50}$ ml^{-1}	3366 ± 23	3360 ± 12	3217 ± 6	3365 ± 2
Influenza A 1:10	1.50×10^4 $CEID_{50}$ ml^{-1}	3343 ± 7	3350 ± 2	3242 ± 4	3245 ± 9
Influenza B	1.50×10^5 $TCID_{50}$ ml^{-1}	3252 ± 12	3252 ± 7	3126 ± 4	3112 ± 6
MERS-coronavirus	1.50×10^5 $TCID_{50}$ ml^{-1}	3368 ± 12	3375 ± 7	3242 ± 11	3241 ± 8
Parainfluenza 1	1.50×10^5 $TCID_{50}$ ml^{-1}	3223 ± 13	3208 ± 6	3088 ± 13	3114 ± 16
Parainfluenza 2	1.50×10^5 $TCID_{50}$ ml^{-1}	3352 ± 18	3366 ± 10	3230 ± 20	3218 ± 11
Parainfluenza 3	1.50×10^5 $TCID_{50}$ ml^{-1}	3109 ± 1	3097 ± 10	2969 ± 17	2982 ± 4
Parainfluenza 4b	1.50×10^5 $TCID_{50}$ ml^{-1}	3374 ± 16	3375 ± 7	3212 ± 6	3223 ± 5
Respiratory syncytial virus	1.50×10^5 $TCID_{50}$ ml^{-1}	3356 ± 19	3356 ± 21	3220 ± 3	3228 ± 18
Rhinovirus	1.40×10^5 $TCID_{50}$ ml^{-1}	3236 ± 9	2945 ± 54	3117 ± 7	2932 ± 54
Rhinovirus 1:10	1.40×10^4 $TCID_{50}$ ml^{-1}	3342 ± 5	3341 ± 7	3235 ± 5	3253 ± 2
SARS-coronavirus	1.50×10^5 $TCID_{50}$ ml^{-1}	3364 ± 6	3365 ± 14	3228 ± 3	3222 ± 12
Bordetella pertussis	1.50×10^6 CFU ml^{-1}	3217 ± 14	3244 ± 16	2981 ± 7	2975 ± 18
Candida albicans	9.96×10^5 CFU ml^{-1}	3249 ± 9	3476 ± 7	3113 ± 8	3096 ± 5
Candida albicans 1:10	9.96×10^4 CFU ml^{-1}	3368 ± 10	3369 ± 2	3234 ± 9	3239 ± 6
Chlamydophila pneumoniae	1.50×10^6 IFU ml^{-1}	3368 ± 26	3360 ± 6	3221 ± 9	3232 ± 7
Haemophilus influenzae	1.50×10^6 CFU ml^{-1}	3231 ± 21	3218 ± 6	3092 ± 9	3095 ± 15
Legionella pneumophila	1.50×10^6 CFU ml^{-1}	3388 ± 2	3371 ± 15	3107 ± 20	3110 ± 14
Mycobacterium tuberculosis	1.50×10^6 CFU ml^{-1}	3244 ± 7	3241 ± 2	2958 ± 7	2964 ± 7
Mycoplasma pneumoniae	1.50×10^6 CFU ml^{-1}	3224 ± 11	3250 ± 6	3091 ± 4	3089 ± 12
Pneumocystis jirovecii	1.50×10^6 nuclei ml^{-1}	3360 ± 6	3372 ± 22	3234 ± 13	3381 ± 7
Pneumocystis jirovecii 1:10	1.50×10^5 nuclei ml^{-1}	3335 ± 2	3349 ± 20	3239 ± 2	3233 ± 8
Pseudomonas aeruginosa	1.50×10^6 CFU ml^{-1}	3360 ± 19	3376 ± 4	2976 ± 4	2970 ± 8
Staphylococcus aureus	1.50×10^6 CFU ml^{-1}	3345 ± 5	3357 ± 10	3234 ± 10	3250 ± 5
Streptococcus pneumoniae	1.50×10^6 CFU ml^{-1}	3124 ± 10	3106 ± 14	2819 ± 31	2857 ± 20
Streptococcus pyogenes	1.50×10^6 CFU ml^{-1}	3378 ± 3	3361 ± 17	3225 ± 9	3219 ± 14
Pooled human nasal wash	N/A	3376 ± 5	3377 ± 5	3208 ± 5	3211 ± 6

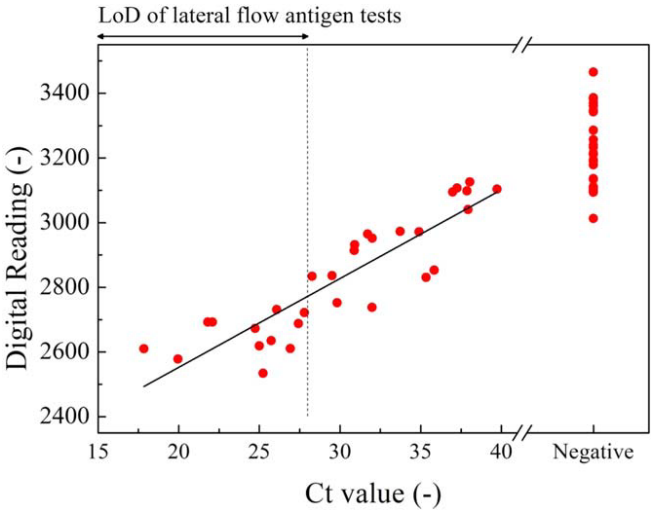

Figure 2. Correlation of digital readings and Ct values using human saliva samples. The Ct value threshold of testing negative was defined as 40.

cross-reactivity or microbial interference due to their genetic similarities. Other common pathogens in the human respiratory system were also covered to mimic the environment for clinical use including 13 viruses, 11 bacteria, 1 fungus, and 1 human pooled nasal wash.

All testing samples were diluted serially to a target concentration with artificial saliva purchased from Pickering Laboratories (Mountain View, CA) as a background matrix. In the cross-reactivity test, organisms were diluted to 1.5×10^5 $TCID_{50}$ ml^{-1} (50% tissue culture infectious dose per milliliter) for virus and 1.5×10^6 PFU ml^{-1} (plaque-forming units per milliliter) for bacteria as suggested by FDA EUA. Prepared samples were then tested with functionalized sensor strips on the PCB and compared with the results of the artificial saliva. In the microbial interference test, FDA suggested diluting to 3×10^5 $TCID_{50}$ ml^{-1} for viruses and 3×10^6 PFU ml^{-1} for bacteria and mixing with an equal volume of 1000 PFU ml^{-1} SARS-CoV-2 inactivated virus VR-1986HK (ATCC). The solution was then tested with the system and compared with the result of 500 PFU ml^{-1} SARS-CoV-2 inactivated virus. If the cross-reactivity or microbial interference was observed, the samples would be further diluted 10 times in artificial saliva and tested until no cross-reactivity or microbial interference was presented.

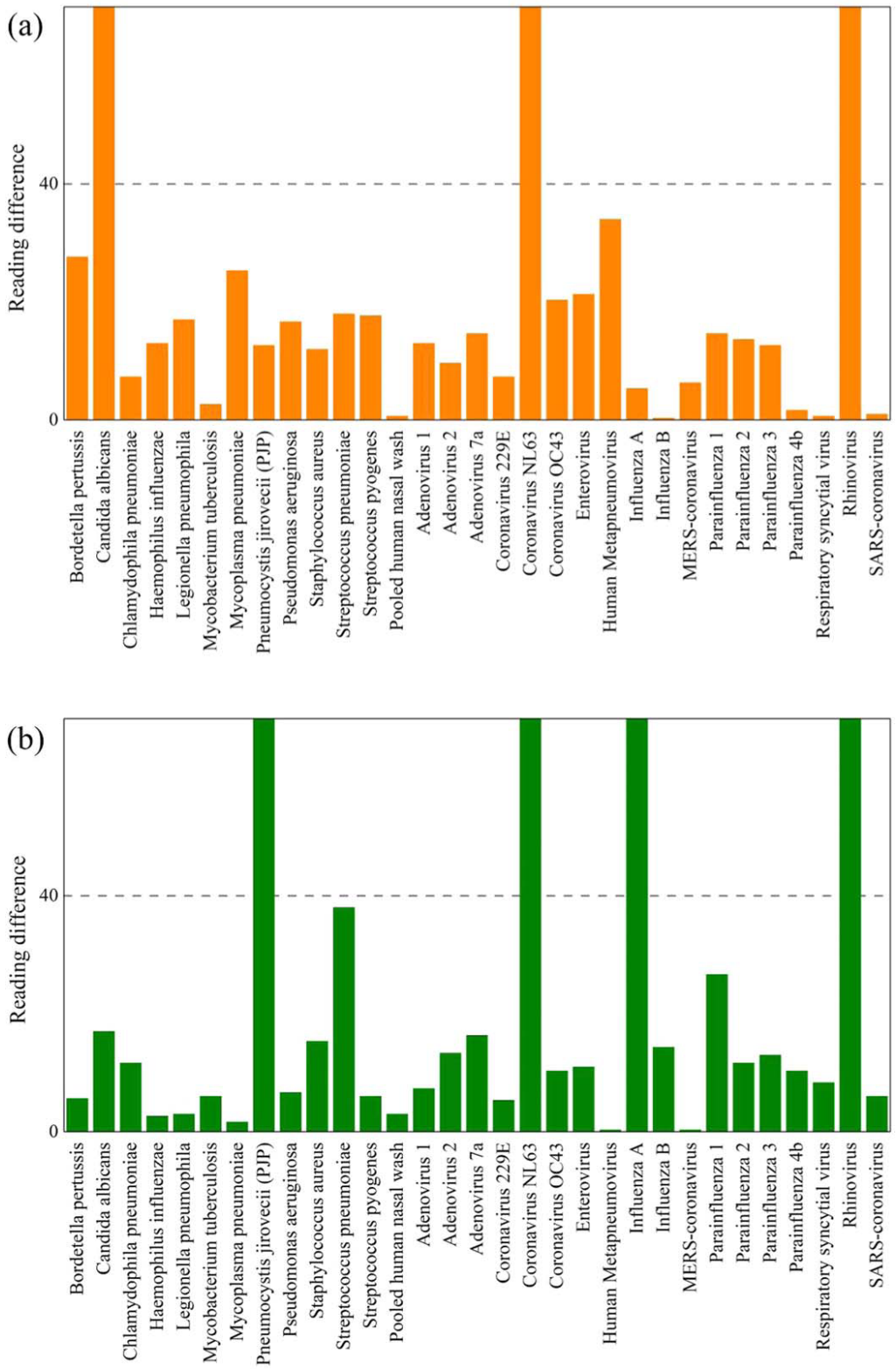

Figure 3. The digital reading difference between (a) artificial saliva and the organism for cross-reactivity tests and (b) SARS-CoV-2 and SARS-CoV-2 with the organism for interference tests.

Results and Discussion

The ability of this sensor technology to detect the SARS-CoV-2 virus in saliva and assess the sensitivity compared with the current gold standard PCR test for detecting the virus was previously reported.[15] The updated correlation between digital readings of our system and PCR results from human saliva samples with various virus concentrations, as well as negative samples without virus, are illustrated in Fig. 2. A linear fitting regression line with a sensitivity of 26/ct value was established based on the data of positive specimens, where the ct value is the cycle threshold number of amplifications to produce a detectable amount of RNA in PCR. Samples with lower ct values have higher virus concentrations,

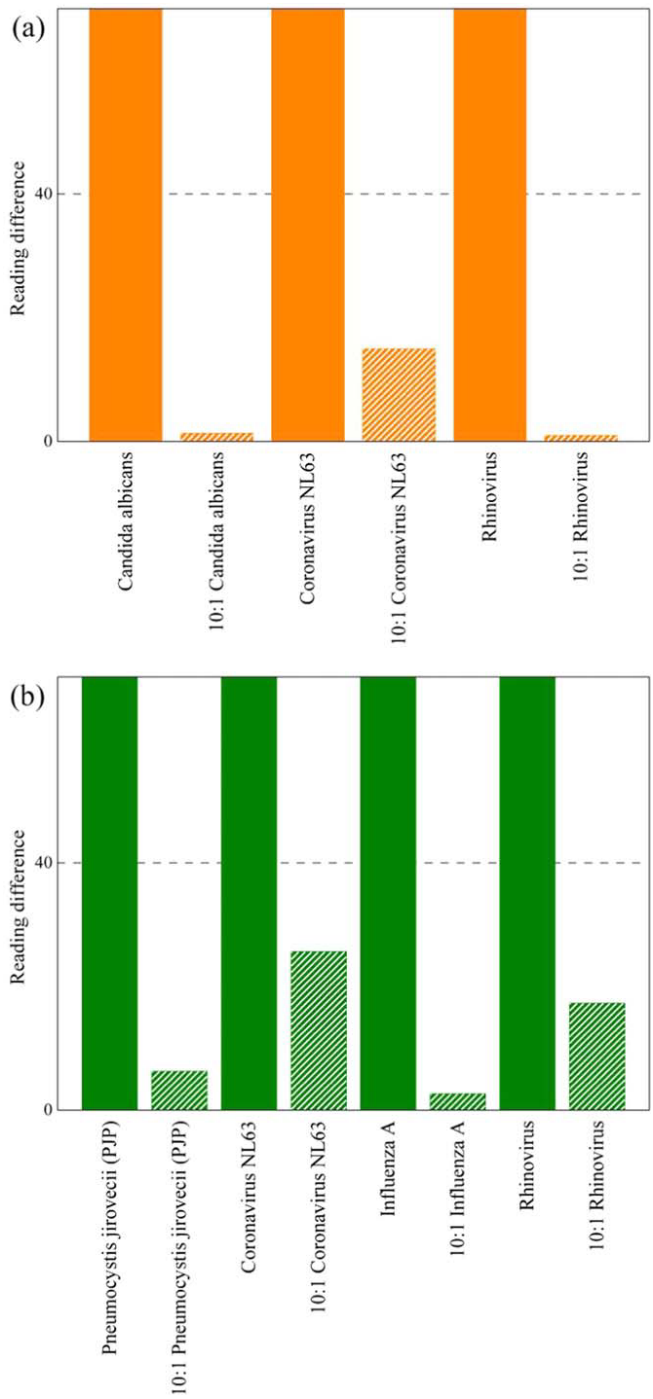

Figure 4. Comparison of the (a) cross-reactivity and (b) microbial interference results before and after 10x dilution.

leading to more captured antigen by the antibodies on the functionalized electrode of the sensor strip. This increased the induced charges to the gate electrode and further increased the drop of the drain voltage of the MOSFET, creating a lower digital reading output. The typical ct values of commercial PCR testing are around 35–37.[16] With a limit of detection (LoD) of 37 ct value, the PCR detects an equivalent of 1000 genome copy numbers per milliliter (gcn ml^{-1}). This value was significantly lower than the LoD of common commercial lateral flow tests of 1×10^6 gcn ml^{-1}[17] and on par with the median LoD of all the US FDA EUA approved virology tests, most of which were performed using the RT-qPCR method.[18]

All of the organisms were analyzed as a contaminant in our system. Table I shows the average digital readings and standard deviations from three replicate tests of the following four conditions: artificial saliva only, the target organism only, SARS-CoV-2 only, and the target organism with SARS-CoV-2.

The cross-reactivity test results, as shown in Fig. 3a, show that the digital reading difference between saliva-only and the organism-only was generally small. Twenty-eight (28) out of 31 samples had a difference smaller than a reasonable error tolerance reading of 40 for the sensor board digital output. This demonstrates that our system has a lower chance of providing false-positive results in the absence of SARS-CoV-2 virus in the testing environment. The microbial interference test results, as illustrated in Fig. 3b, demonstrate that the differences in the digital readings between SARS-CoV-2 only and the SARS-CoV-2 with the organism for 27 out of 31 samples were also smaller than the error tolerance. This further indicates the sensitivity of our system is not affected by these organisms.

Although not all of the organisms passed the evaluation for cross-reactivity and microbial interference in their original concentration, the negative effects were no longer detected after an additional one order of magnitude dilution. The comparison of test results of the original concentration and a 10 times dilution with artificial saliva is illustrated in Figs. 4a and 4b. All of the 5 organisms with either cross-reactivity or microbial interference presented in the original concentration have a digital reading difference below 40 once diluted. This value is considered acceptable with the standard of FDA EUA.

Conclusions

The continuous mutation and infection of SARS-CoV-2 are wreaking havoc on global economies. The current approach of seeking co-existence with the virus leads to the ever-rising demand for novel detection methods. These new results on effects of common contaminants encountered during testing further extends emphasizes the feasibility of our approach and its compliance with the requirement of the FDA EUA guidelines for cross-reactivity testing. All the 31 contaminants identified in the FDA EUA, including common viruses, bacteria, and fungus in the human respiratory system, along with high interference risk groups of coronaviruses from the same generic family with SARS-CoV-2, demonstrated no signs of cross-reactivity or microbial interference with our detection system. This proves our sensor's potential to abide by the policies and regulation for clinical use and marks a step forward towards commercialization of this product.

Acknowledgments

The work performed in UF was supported by Houndstoothe Analytics. The authors at National Yang Ming Chiao Tung University, Hsinchu 30010, Taiwan would like to thank the Ministry of Science and Technology, Taiwan, for their financial support under the grants MOST 107-2918-I-009-010 and 108-2636-E-009-008.

ORCID

Chao-Ching Chiang https://orcid.org/0000-0002-0447-8170
Stephen J. Pearton https://orcid.org/0000-0001-6498-1256

References

1. G. Rong, Y. Zheng, Y. Chen, Y. Zhang, P. Zhu, and M. Sawan, *Reference Module in Biomedical Sciences*, **3**, 17 (2021).
2. M. Shen, Y. Zhou, J. Ye, A. A. Abdullah Al-Maskri, Y. Kang, S. Zeng, and S. Cai, *J Pharm Anal*, **10**, 97 (2020).
3. B. Udugama, P. Kadhiresan, H. N. Kozlowski, A. Malekjahani, M. Osborne, V. Y. C. Li, H. Chen, S. Mubareka, J. B. Gubbay, and W. C. W. Chan, *ACS Nano*, **14**, 3822 (2020).
4. M. Platten, D. Hoffmann, R. Grosser, F. Wisplinghoff, H. Wisplinghoff, G. Wiesmuller, O. Schildgen, and V. Schildgen, *Viruses*, **13**, 1459 (2021).
5. D. Sung and J. Koo, *Biomed Eng Lett*, **11**, 85 (2021).
6. G. Seo et al., *ACS Nano*, **14**, 5135 (2020).

7. J. Li, D. Wu, Y. Yu, T. Li, K. Li, M. M. Xiao, Y. Li, Z. Y. Zhang, and G. J. Zhang, *Biosens. Bioelectron.*, **183**, 113206 (2021).
8. L. Wang et al., *Nat. Biomed. Eng.*, **6**, 276 (2022).
9. S. Kumar, R. K. Chauhan, and M. Kumar, *Silicon* (2022).
10. M. Xian et al., *J Vac Sci Technol B Nanotechnol Microelectron*, **39**, 033202 (2021).
11. S. Y. Lu, S. S. Shan, J. Yang, C. W. Chang, F. Ren, J. Lin, S. Pearton, and Y. T. Liao, *Annual International Conference of the IEEE Engineering in Medicine and Biology Society. IEEE Engineering in Medicine and Biology Society. Annual International Conference* p. 5761 (2019).
12. P. H. Carey, J. Yang, F. Ren, C.-W. Chang, J. Lin, S. J. Pearton, B. Lobo, and M. E. Leon, *J. Electrochem. Soc.*, **166**, B708 (2019).
13. J. Yang, P. Carey, F. Ren, Y.-L. Wang, M. L. Good, S. Jang, M. A. Mastro, and S. J. Pearton, *Appl. Phys. Lett.*, **111**, 202104 (2017).
14. J. Yang, P. Carey, F. Ren, M. A. Mastro, K. Beers, S. J. Pearton, and I. I. Kravchenko, *Appl. Phys. Lett.*, **113**, 032101 (2018).
15. C.-W. Chiu et al., *J. Vac. Sci. Technol. B*, **40**, 023204 (2022).
16. S. Pickering et al., *Lancet Microbe,*, **2**, e461 (2021).
17. A. I. Cubas-Atienzar et al., *Sci. Rep.*, **11**, 18313 (2021).
18. M. J. MacKay et al., *Nat. Biotechnol.*, **38**, 1021 (2020).